Asymmetric Berry-Phase Interference Patterns in a Single-Molecule Magnet

H. M. Quddusi,[1] J. Liu,[2] S. Singh,[1] K. J. Heroux,[4] E. del Barco,[1] S. Hill,[3] and D. N. Hendrickson[4]

[1]*Department of Physics, University of Central Florida, Orlando, Florida 32816, USA*
[2]*Department of Physics, University of Florida, Gainesville, Florida 32611, USA*
[3]*National High Magnetic Field Laboratory and Department of Physics, Florida State University, Tallahassee, Florida 32310, USA*
[4]*Department of Chemistry and Biochemistry, University of California at San Diego, La Jolla, California 92093, USA*

A Mn_4 single-molecule magnet displays asymmetric Berry-phase interference patterns in the transverse-field (H_T) dependence of the magnetization tunneling probability when a longitudinal field (H_L) is present, contrary to symmetric patterns observed for $H_L = 0$. Reversal of H_L results in a reflection of the transverse-field asymmetry about $H_T = 0$, as expected on the basis of the time-reversal invariance of the spin-orbit Hamiltonian which is responsible for the tunneling oscillations. A fascinating motion of Berry-phase minima within the transverse-field magnitude-direction phase space results from a competition between noncollinear magnetoanisotropy tensors at the two distinct Mn sites.

PACS numbers: 75.50.Xx, 75.45.+j, 76.30.-v

Almost two decades of research have established single-molecule magnets (SMMs) as prototype systems for understanding fundamental quantum phenomena associated with nanoscale magnetism [1,2], as well as demonstrating their potential for future applications [3]. The most important characteristics of SMMs can be modeled reliably using a giant-spin approximation (GSA) whereby the molecule is treated as a rigid magnetic unit with total spin, S, weakly interacting with its enviroment. Indeed, this model accounts for the essential features of the quantum tunneling of magnetization (QTM) observed in these molecules, as well as its quenching due to Berry-phase interference (BPI) resulting from different tunneling trajectories [4–6]. However, the GSA ignores the internal couplings within a SMM, thereby completely failing to account for QTM transitions that involve fluctuations of the total spin of the molecule [7–9], or otherwise obscuring intrinsic relationships that exist between QTM selection rules and the underlying molecular structure [10]. In a recent interesting example, it was demonstrated that a tilting of the zero-field splitting (zfs) tensors in a triangular Mn_3^{III} SMM (lowering the symmetry of the spin Hamiltonian from C_6 to C_3) results in new QTM selection rules and strongly affects the transverse-field dependence of the remaining forbidden QTM resonances [10]. These observations likely explain the absence of QTM selection rules in most SMMs studied to date, since internal dipolar fields and/or weak sample disorder are often sufficient to cause observable relaxation at resonances otherwise forbidden by symmetry. A detailed understanding of these and related phenomena has mostly been facilitated by studies of low nuclearity SMMs [11,12], where exact diagonalization of the multispin Hamiltonian enables consideration of the internal degrees of freedom of the molecule.

In this Letter, we focus on the QTM relaxation associated with a centro-symmetric mixed-valent $Mn_2^{II}Mn_2^{III}$ complex which shows an asymmetric BPI pattern with respect to the polarity of the transverse component of the applied field ($H_T \perp$ magnetic easy axis). We show that this behavior results from a competition between noncollinear magneto-anisotropy tensors at the two crystallographically distinct Mn ions, which is also responsible for an unusual motion of the Berry-phase minima within the transverse-field magnitude-direction phase space. We show how the asymmetry can be inverted upon reversal of the longitudinal field ($H_L \parallel$ easy axis); i.e., the BPI pattern is invariant with respect to a full inversion of the applied field, consistent with the time-reversal symmetry of the underlying zero-field Hamiltonian.

The $[Mn_4(Bet)_4(mdea)_2(Hmdea)_2](BPh_4)_4$ complex (henceforth Mn_4-Bet) crystallizes in the triclinic $P\bar{1}$ space group with half the molecule in the asymmetric unit; the other half is generated via inversion, resulting in the four Mn ions lying in a plane (the molecular plane), with the Mn^{III} Jahn-Teller (JT) axes oriented along the Mn^{III}-N bonds, which lie 122.61 degrees out of this plane, i.e., roughly perpendicular to the molecular plane [13,14]. There are no solvent groups in the lattice and the four BPh_4^- anions enhance isolation, resulting in extremely clean x-ray diffraction and EPR data [14,15]. A sketch of the Mn_4 core, where the magnetic axes are indicated, is inset to Fig. 1. Magnetic and EPR measurements performed at relatively high temperatures ($T > 2$ K) suggest a spin $S = 9$ ground state, and that Mn_4-Bet is a SMM with a barrier of ~20 K [14].

A high-sensitivity micro-Hall effect magnetometer, a He^3/He^4 dilution fridge and a 3D vector superconducting magnet were employed to record magnetization hysteresis curves as a function of a magnetic field applied parallel to the easy axis of the molecules [16], at temperatures down to 35 mK. The results are shown in Fig. 1, where extremely sharp QTM resonances ($k = 0$, 1, and 2), spaced by
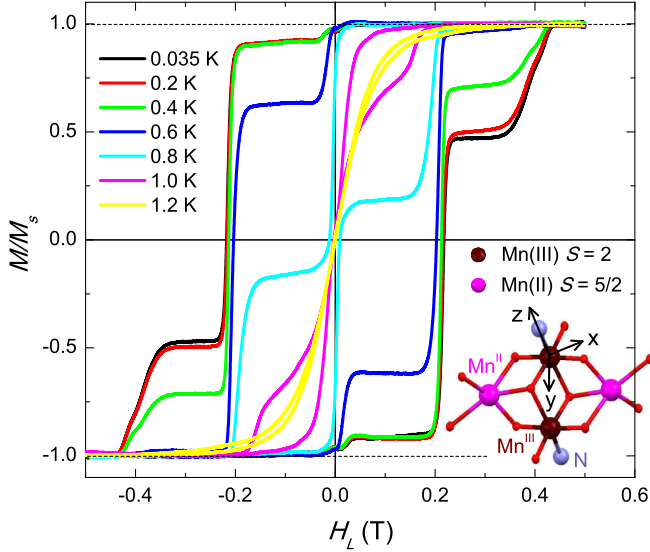
FIG. 1 (color online).   Hysteresis loops recorded as a function of H_L at different temperatures. The inset shows the relevant magnetic centers (i.e., Mn^{II}, Mn^{III}, N and O) at the core of the Mn_4-Bet unit. The principal magnetic axes of the molecule are indicated, with the easy (z) axis determined by the JT elongation associated with the Mn^{III} ions (Mn^{III}-N line, see main text); the y axis lies in the plane defined by the two Mn^{III} ions and their JT axes.
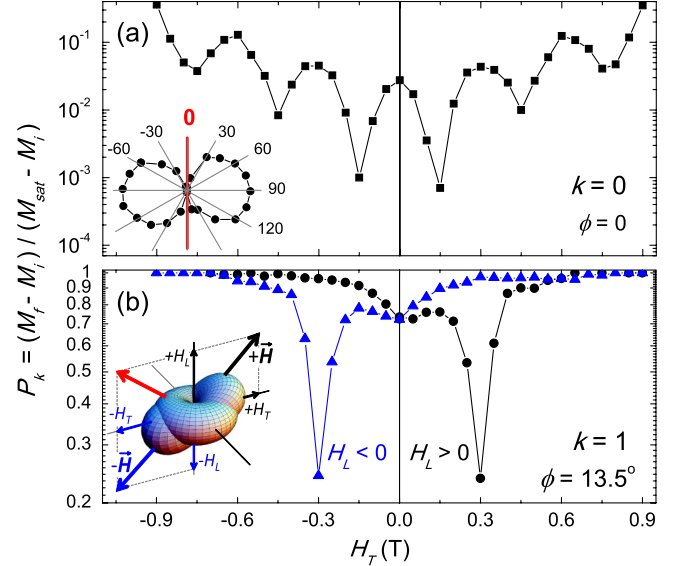

FIG. 2 (color online).   Modulation of the QTM probabilities for resonances $k = 0$ (a) and $k = 1$ (b) as a function of H_T applied at different angles, ϕ, within the hard plane of the Mn_4-Bet SMM [18]. The inset to (a) illustrates the two-fold angular modulation of P_0 for $H_T = 0.2$ T, providing clear evidence for a significant 2nd-order rhombic anisotropy. The asymmetry of the BPI pattern of oscillations in resonance $k = 1$ is inverted upon reversal of H_L. The inset to (b) illustrates the classical anisotropy barrier generated by the noncollinear zfs tensors (see main text for explanation) and the different perspectives resulting from permutations of $\pm H_T$ and $\pm H_L$.

$\Delta H_L \approx 0.21$ T, confirm the high quality of the crystal. Within the GSA, this spacing corresponds to an axial zfs parameter, $D = -0.28$ K ($g = 2$). The observed blocking and crossover temperatures are ~ 1.2 and ~ 0.2 K, respectively. A transverse field was subsequently employed in order to study the symmetry of the QTM in resonances $k = 0$ and $k = 1$. Figure 2(a) shows the modulation of the QTM probability, $P_k = (M_f - M_i)/(M_{sat} - M_i)$ [17], for resonance $k = 0$, as a function of H_T applied along the magnetic hard axis ($\phi = 0°$). This angle, which lies $\sim 30°$ away from one of the crystal faces, was deduced from the twofold modulation of P_0 as a function of the orientation, ϕ, of a 0.2 T transverse field within the hard plane [see inset to Fig. 2(a)] [18].

The P_0 oscillations in Fig. 2(a) correspond to BPI, with minima at regularly spaced field values ($\Delta H_T = 0.3$ T). A maximum in P_0 is found at $H_T = 0$, as expected for an integer spin value. Within the GSA, $\Delta H_T = 2k_B(2E[E + D])^{1/2}/g\mu_B$ [19], yielding a 2nd-order rhombic zfs parameter, $E = \pm 60$ mK. Note that the regularly spaced $k = 0$ BPI minima are invariant under inversion of H_T; i.e., they are symmetric with respect to $H_T = 0$. Interestingly, this is not the case in resonance $k = 1$, for which the behavior of the QTM probability is very different. This can be seen in Fig. 2(b), which illustrates the dependence of P_1 on H_T, for $\phi = 13.5°$ (the angle for which the first BPI minimum at $H_T = 0.30$ T is the sharpest). In fact, for resonance $k = 1$, different BPI minima appear at different field orientations, ϕ, of the transverse field within the xy (hard) plane of the molecule (see Fig. 3)

[18]; i.e., the first minimum ($H_T = 0.3$ T) appears at $\phi = 13.5°$, while the second ($H_T = 0.6$ T) occurs at $\phi = 6°$, contrary to what is found for the $k = 0$ resonance (all P_0 minima are seen most clearly at $\phi = 0°$). Such behavior has been predicted theoretically [20,21], though never observed experimentally.

Before considering this aspect in detail, we first discuss the asymmetric nature of the BPI oscillation pattern in resonance $k = 1$. As seen clearly in Fig. 2(b), reversal of the longitudinal field, H_L, results in a reflection of the P_1 BPI pattern about $H_T = 0$. In other words, the BPI minima *are* in fact invariant under a full magnetic field inversion, as required on the basis of the time-reversal invariance of the spin-orbit Hamiltonian responsible for this physics. As noted above, the symmetries of BPI patterns must respect the symmetry of the zero-field spin Hamiltonian. If one considers only 2nd-order zfs within the GSA, then the resulting Hamiltonian necessarily belongs to the orthorhombic point group and possesses the following symmetry elements: (i) three mutually orthogonal twofold rotation axes (x, $y \& z$); (ii) three mutually orthogonal mirror planes (xy, $xz \& yz$); and (iii) an inversion center. (ii) guarantees invariance with respect to reversal of H_T; i.e., it enforces symmetric BPI patterns, irrespective of whether a longitudinal field is applied ($k > 0$) or not ($k = 0$). As we show below, one must break the xy mirror symmetry in order to

obtain asymmetric BPI patterns with respect to inversion of H_T. In this case, reversal of H_L results in different patterns; the time-reversal symmetry then guarantees that these two patterns are mirror images. Nevertheless, no matter how many spatial symmetries are broken, the time-reversal invariance of the spin-orbit interaction guarantees that the BPI minima should be invariant under a full reversal of the applied field, i.e., simultaneous reversal of H_L and H_T, as we have confirmed experimentally.

It is possible to reproduce the essential features of the experiments by introducing 4th-order terms into the GSA; the xy mirror symmetry can then be broken by rotating the coordinate frames of the 2nd and 4th-order tensors. Interestingly, this approach also reproduces the complex motion of the P_1 minima within the $H_T - \phi$ phase-space shown in Fig. 3. However, a complete GSA analysis for Mn_4-Bet requires many parameters and provides little insight, while the same physics can be naturally understood within a multispin description which considers the internal structure of the Mn_4-Bet molecule. Note that the emergence of significant higher-order anisotropy terms within the GSA is a manifestation of mixing of the ground spin state with excited states, which can only be captured within a multispin model [11,12]. In this context, the xy mirror symmetry may be trivially broken by rotating (tilting) the zfs tensors at the two inequivalent magnetic sites in the molecule so that their local z axes no longer coincide (this is similar to the case of the Mn_3^{III} SMM discussed in the introduction [10,22]).
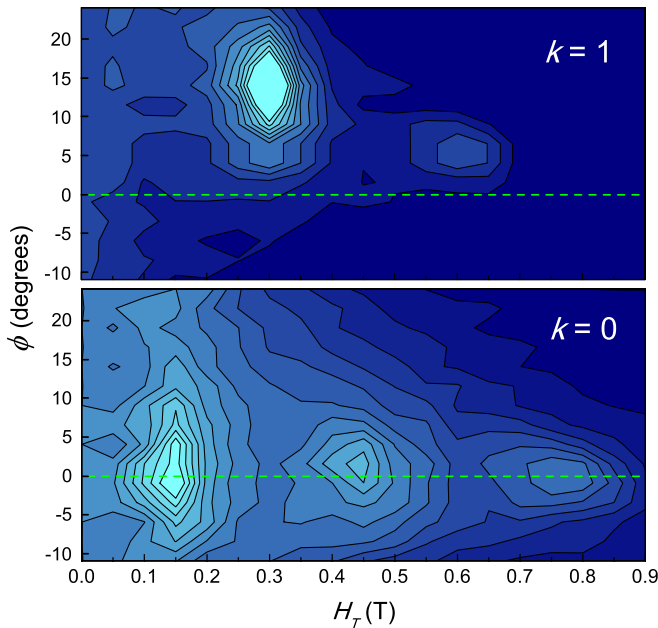
To explain the experimental findings we have diagonalized the multispin Hamiltonian, where the four Mn ions are coupled according to the sketch in Fig. 4(a).

$$H = \sum_{i=1}^{3}(\vec{s}_i \cdot \tilde{R}_i^T \cdot \tilde{d}_i \cdot \tilde{R}_i \cdot \vec{s}_i - g\mu_B \vec{s}_i \cdot \vec{B})$$
$$+ \sum_{i,j(i>j)}(\vec{s}_i \cdot \tilde{J}_{i,j} \cdot \vec{s}_j - \frac{\mu_0(g\mu_B)^2}{4\pi r_{i,j}^3}\vec{s}_i \cdot \tilde{\Delta}_{i,j} \cdot \vec{s}_j). \quad (1)$$

The first term represents the local anisotropy of the ith ion, $\tilde{d}_i$ being the 2nd-order zfs tensor ($d_{i,xx} = e_i$, $d_{i,yy} = -e_i$, and $d_{i,zz} = d_i$, with d_i and e_i representing the axial and rhombic anisotropies, respectively); the $\tilde{R}_i$ are Euler matrices (defined by Euler rotation angles α_i, β_i & γ_i) specifying the orientations of these tensors. The second term is the Zeeman coupling to the applied field, where we assume an isotropic Landé factor, $g = 2.00$. The third and fourth terms represent the exchange and dipolar interactions, respectively. These terms are also time-reversal invariant, and do not change any of the preceding arguments. As depicted in Fig. 4(a), three independent near-neighbor exchange coupling constants, J_a, J_b and J_c, are considered: $J_{1,2} = J_{3,4} = J_a$, $J_{2,3} = J_{1,4} = J_b$, $J_{2,4} = J_c$ and $J_{1,3} = 0$. The dipolar matrix, $\tilde{\Delta}_{i,j}$ has been chosen to exactly reproduce all of the dipolar couplings within the molecule, with no fitting parameters.

Figure 4(b) plots the locations of BPI minima obtained via diagonalization of Eqn. (1) (solid red symbols). This simulation, which takes into account the small
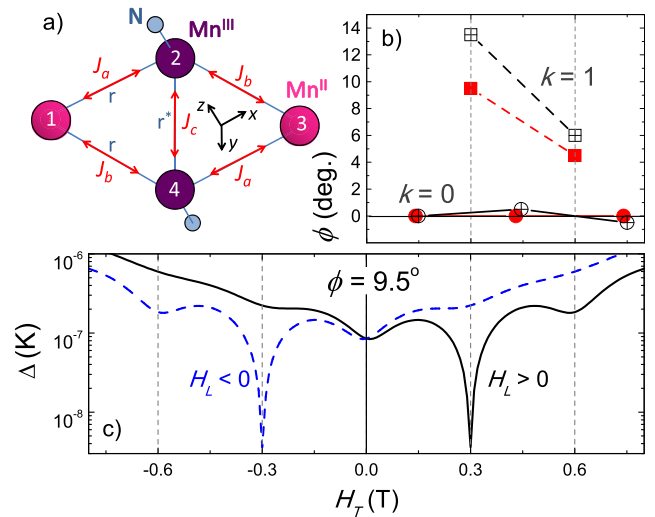

FIG. 3 (color online). Contour plots of the QTM probabilities for resonances $k = 0$ and $k = 1$ as a function of H_T and ϕ. All of the $k = 0$ minima lie approximately along the $\phi = 0°$ axis, whereas the $k = 1$ minima appear at different orientations for different H_T values.

FIG. 4 (color online). (a) Sketch of the Mn_4 core indicating the interaction parameters used to explain the results. (b) Measured (open black symbols) and calculated (solid red symbols) ϕ/H_T-dependence of the BPI minima for resonances $k = 0$ (circles) and 1 (squares) obtained from Eqn. (1). (c) Calculated tunnel splittings for resonance $k = 1$, for $\phi = 9.5°$, as a function of H_T for $H_L > 0$ (continuous black line) and $H_L < 0$ (discontinuous blue line).

misalignment of the experimental field rotation plane [18], employed the following parameters: $d_2 = d_4 = -4.99$ K and $e_2 = e_4 = 0.82$ K, with the easy and hard anisotropy axes along z ($\alpha_2 = 0$) and x ($\beta_2 = 0$), respectively; $d_1 = d_3 = -0.67$ K & $e_1 = e_3 = 0$, with the axes rotated with respect to the central spin by identical Euler angles $\alpha_{1,3} = 45°$, $\beta_{1,3} = 0°$ (as required by inversion symmetry); γ being zero for all ions; finally, isotropic ferromagnetic exchange constants $J_a = -3.84$ K, $J_b = -1.20$ K and $J_c = -3.36$ K are used. It should be stressed that these parameters are additionally constrained by the locations of hysteresis loop steps (Fig. 1) and extensive angle-dependent EPR measurements [15]. Moreover, the obtained anisotropy values for the Mn^{III} ions are very similar to related Mn^{III} complexes [10], while the $d_{1,3}$ value lies within the bounds reported for other Mn^{II} systems [23]. The quantitative agreement with experiment is also excellent. The motion of the P_1 minima can be understood as a result of the competition between different anisotropic interactions within the molecule, without a need to invoke unphysical 4th and higher-order anisotropies. Importantly, the angular positions (ϕ) of the $k = 1$ minima move with H_T, while the $k = 0$ minima remain stationary, as found experimentally (Fig. 3).

Finally, the multispin model perfectly reproduces the H_T asymmetry of the $k = 1$ BPI pattern. As seen in Fig. 4(c), the asymmetry is reversed upon inversion of H_L, as required by the time-reversal invariance of the anisotropic interactions in Eq. (1), and observed experimentally [Fig. 2(b)]. The crucial ingredient is the tilting of the zfs tensors of the external spins, s_1 & s_3, relative to the central spins s_2 & s_4, so that the xy mirror symmetry is broken. This is illustrated in the inset to Fig. 2(b), where one observes that the classical energy landscape is invariant under full field inversion (blue vs black arrows), while this is not the case when only H_T is reversed (red vs black arrows). The Euler angle $\alpha_{1,3} = 45°$ results in a significant projection of the relatively weak anisotropy associated with the Mn^{II} ions into the hard (xy) plane. This, together with the finite $e_{2,4}$ parameters and the dipolar interactions, results in competing transverse interactions and to the complexity of the BPI patterns observed in Fig. 3. We note that the dipolar interaction has a very significant effect on the energy levels of the molecule: the zfs within the $S = 9$ multiplet varies by as much as 10% when dipolar interactions are omitted, and the location of the $k = 1$ QTM step is shifted by ~ 0.02 T.

We conclude by noting that asymmetric BPI patterns have been seen in other centro-symmetric SMMs for which a clear explanation has been lacking [7,9,24]. The present results may help shed light on the effect that symmetric anisotropic interactions can have in magnetic systems with inversion symmetry, where a net antisymmetric interaction is strickly forbidden. The present work clearly demonstrates how studies of simple low nuclearity systems can address fundamental symmetry considerations related to QTM in molecular nanomagnetism.

[1] E. M. Chudnovsky and J. Tejada, *Macroscopic Quantum Tunneling of Magnetic Moment* (Cambridge University Press, Cambridge, England, 1998).
[2] D. Gatteschi, R. Sessoli, J. Villain, *Molecular Nanomagnets* (Oxford Univ. Press, Oxford, 2008).
[3] M. N. Leuenberger and D. Loss, Nature (London) **410,** 789 (2001).
[4] W. Wernsdorfer and R. Sessoli, Science **284,** 133 (1999).
[5] E. del Barco, A. D. Kent, E. M. Rumberger, D. N. Hendrickson, and G. Christou, Phys. Rev. Lett. **91,** 047203 (2003).
[6] M. S. Foss-Feig and J. R. Friedman, Europhys. Lett. **86,** 27002 (2009).
[7] C. M. Ramsey *et al.*, Nature Phys. **4,** 277 (2008).
[8] S. Carretta *et al.*, Phys. Rev. Lett. **100,** 157203 (2008).
[9] S. Bahr *et al.*, Phys. Rev. B **78,** 132401 (2008).
[10] J. J. Henderson *et al.*, Phys. Rev. Lett. **103,** 017202 (2009).
[11] S. Hill *et al.*, Dalton Trans. **39,** 4693 (2010).
[12] A. Wilson *et al.*, Phys. Rev. B **74,** R140403 (2006).
[13] The CIF file (CCDC 790437) has been deposited with the Cambridge Crystallographic Data Centre (CCDC). These data can be obtained free of charge from the CCDC via http://www.ccdc.cam.ac.uk/cgi-bin/catreq.cgi.
[14] K. J. Heroux *et al.* (to be published).
[15] See supplemental material at http://link.aps.org/supplemental/10.1103/PhysRevLett.106.227201 for the high-frequency EPR spectra recorded on this complex, as well as fits to the multispin Hamiltonian given in the text.
[16] The magnetic axes were determined experimentally from the angular field behavior of the QTM resonances.
[17] M_i and M_f are the magnetizations before and after the resonance, respectively. M_{sat} is the saturation value.
[18] We note that there was a small ($\sim 3°$) misalignment of the field rotation plane during the measurements. This slightly influences, but is not the primary cause of, the BPI minima motion. Simulations demonstrate that similar results are obtained when H_T is rotated exactly within the xy plane, for which the $k = 1$ first and second BPI minima are found at $\phi = 7.5°$ and $\phi = 3°$, respectively.
[19] A. Garg, Europhys. Lett. **22,** 205 (1993).
[20] E. del Barco *et al.*, J. Low Temp. Phys. **140,** 119 (2005).
[21] K. Hijii and S. Miyashita, Phys. Rev. B **78,** 214434 (2008).
[22] J. Liu *et al.* (unpublished).
[23] J. Krzystek, A. Ozarowski, and J. Telser, Coord. Chem. Rev. **250,** 2308 (2006).
[24] E. del Barco *et al.*, Phys. Rev. B **82,** 104426 (2010).
[25] http://hpc.ufl.edu